Supplementary Information: Hyperspectral interference tomography of nacre

Jad Salman[1], Cayla A. Stifler[2], Alireza Shahsafi[1], Chang-Yu Sun[2], Stephen C. Weibel[3], Michel Frising[1], Bryan E. Rubio-Perez[1], Yuzhe Xiao[1], Christopher Draves[3], Raymond A. Wambold[1], Zhaoning Yu[1,2], Daniel C. Bradley[2], Gabor Kemeny[3], Pupa U. P. A. Gilbert[2,4,5,6,7], Mikhail A. Kats[1,2,5]

[1]Department of Electrical and Computer Engineering, [2]Department of Physics University of Wisconsin–Madison, Madison WI 53706. [3]Middleton Spectral Vision, Middleton, WI 53562. [4]Department of Chemistry, [5]Department of Materials Science and Engineering, [6]Department of Geoscience, University of Wisconsin–Madison, Madison WI 53706. [7]Chemical Sciences Division, Lawrence Berkeley National Laboratory, Berkeley, CA 94720.

1. Structural color dependence on angle

Optical interference effects in thin-film assemblies are dependent on the thicknesses and refractive indices of the films and the angle of the incident light with respect to the structure. Figure S1 shows the structural color of nacre produced by two different mollusk species: *Haliotis rufescens* and *Haliotis iris*. The iridescent colors are clearly dependent on the viewing angle, as seen when the angle of incidence is changed between the illuminating source (sunlight) and the camera. As the samples are tilted from near-normal to oblique angles (Fig. S1 a-c, d-f) the range of reflected colors shift from predominately red, orange, and yellow (longer wavelengths) to greens, blues, and violets (shorter wavelengths).

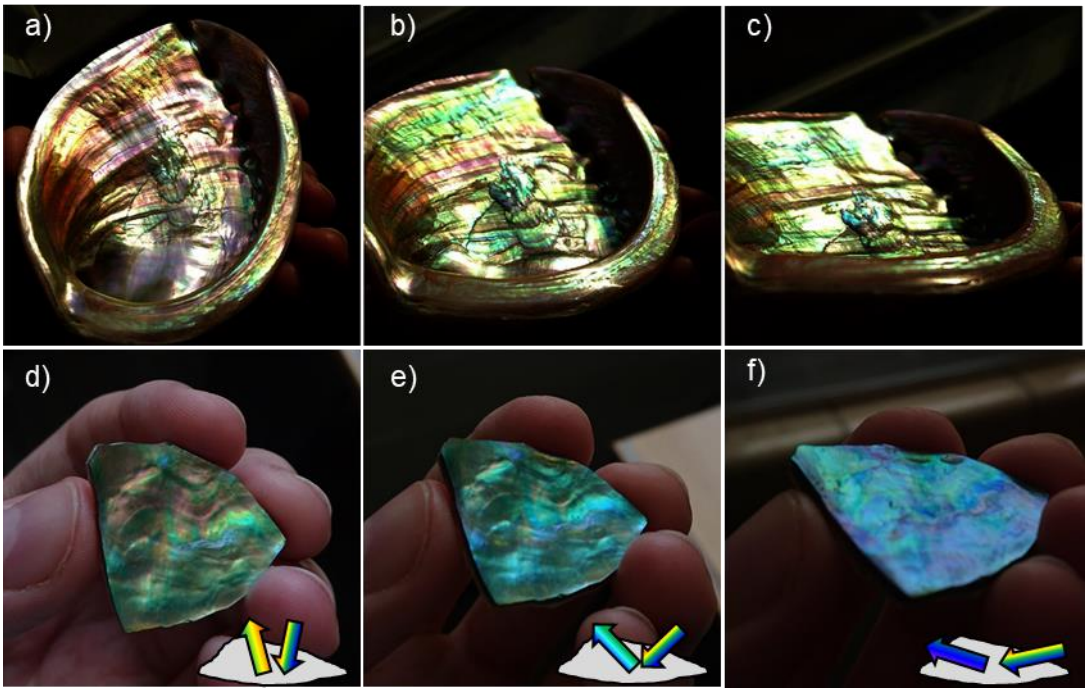

Figure S1: Structural-color dependence on the incidence and reflection angles. Nacre samples from *Haliotis rufescens* (a-c) and *Haliotis iris* (d-f) were imaged at various incidence angles (left to right) while illuminated with sunlight.

Interference enables the high reflectivity in Bragg reflectors. In an ideal Bragg reflector, alternating lossless dielectric materials are stacked with thicknesses corresponding to $\frac{\lambda_o}{4n_{1,2}}$ (when designed for normal incidence), where λ_o is the central wavelength for constructive interference in reflection and $n_{1,2}$ corresponds to the refractive index of the high- or low-index layers, respectively. In Fig. S2a, the simulated reflectance spectrum for a 50-layer Bragg reflector is shown. The thin-film assembly was designed to have peak reflectance at λ_o = 600 nm at normal incidence and used alternating high- and low-index materials equivalent to nacre's aragonite crystals (n_1 = 1.63) and organic polymer (n_2 = 1.43). Thus, the thickness of the high- and low-index layers were 92 and 105 nm, respectively. As the angle of incidence transitions from normal to oblique, the central wavelength shifts towards shorter wavelengths.

The stratified structure of nacre is essentially a Bragg reflector with disorder in the layer thicknesses. Figure S2b shows the reflectance spectrum for the same Bragg reflector as in S2a but with a 20 nm standard deviation in the thicknesses from a mean set to the ideal thicknesses for the high- and low-index layers. The reflectance spectra shown are the average of 30 simulations with randomly distributed disorder in the layer thicknesses. The angle dependence of the Bragg peak remains, though the amplitude is reduced and the peak is broadened compared to the perfect Bragg reflector.

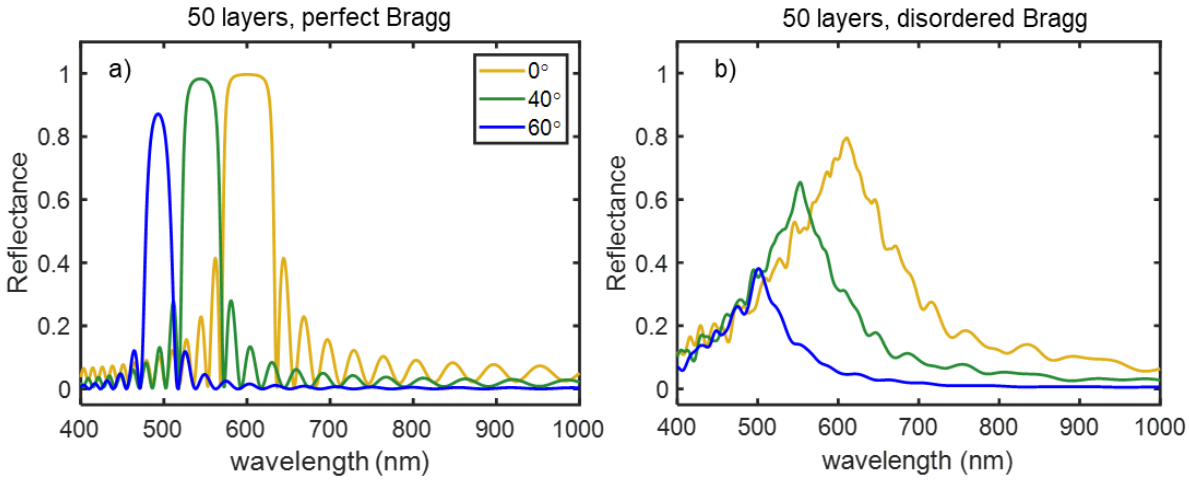

Figure S2: Bragg reflector without (a) and with (b) disorder. a) Transfer-matrix method calculation of the reflectance from a 50-layer perfect Bragg reflector designed with central wavelength λ_o = 600 nm for normal incidence. The refractive indices, n_1 and n_2, are 1.63 and 1.43, respectively. b) The calculated reflectance spectrum of a 50-layer disordered Bragg reflector for which the standard deviation of the thicknesses is 20% of the perfect thickness from the ideal condition. These spectra are the average of 30 randomly generated disordered stacks.

2. Impact of model assumption on fitting

We assumed the constituents of nacre to be dispersionless and lossless throughout the visible and near infrared, and consistent with values reported in literature. The aragonite tablets were assigned refractive index $n_{aragonite}$ = 1.63, and the organic polymer was assigned refractive index $n_{organic}$ = 1.43. The real constituent materials likely have some dispersion across the wavelength range of interest, and a range of literature values for chitin proteins refractive indices have been reported. To determine the potential impact to our modeling of nacre, we calculated the individual impact on the final mean tablet thickness (MTT) fittings given reasonable variations in the refractive indices of the aragonite and organic layers, as well as systematic variations in the angle of incidence.

Table S1 details the impact to MTT fits due to deviations in the modeling assumptions. First, the baseline calculation sets $n_{aragonite} = 1.63$, $n_{organic} = 1.43$, and the angle of incidence (AOI) to 30°, with the remaining model assumptions the same as outlined in the main text. A set of reflectance spectra, R, are generated for all MTT (150 – 600 nm) and degree of disorder in tablet thickness (TT), which is the standard deviation, σ (5 – 75 nm). Then, for each variation in the refractive index or AOI parameters, a new set of reflectance spectra, R', is calculated within the same MTT and σ parameter space. The impact from each individual parameter variation is determined by performing a fit (see Fig. 2 in the main text) between R and R' and extracting an expected MTT. The difference between baseline and the expected MTT fits is a measure of the impact of a given parameter variation on the final MTT. The largest impact on MTT was when setting $n_{aragonite} = 1.53$, the refractive index of aragonite along the c-axis, with an approximately 30 nm change to the MTT. Using R' values to fit the MTT using measured nacre spectra shows a similar impact on the MTT.

Table S1: Impact on the calculated mean tablet thickness (MTT) from model variations. The impact is quantified as the magnitude in the average of the differences in MTT.

	$n_{aragonite} = 1.53$	$n_{aragonite} = 1.68$	$n_{organic} = 1.4$	$n_{organic} = 1.73$	AOI = 35°	AOI = 25°
Simulated [a] |ΔMTT| (nm)	27	11	6	2	9	3
Measured [b] |ΔMTT| (nm)	25	11	10	1	6	5

[a] The difference in MTT between the fitting of *R* to *R'* datasets

[b] The difference in MTT between the fitting of measured nacre reflectance to *R* and *R'*

3. Optical modeling using SEM-measured layer thicknesses to determine penetration depth

Light interacting with nacre can be scattered and attenuated by inhomogeneities and losses in the material. As described in the main text, hyperspectral interference tomography (HIT) restricts the measurement to specular reflections. However, the maximum depth at which the specular light penetrates the nacre and is then reflected and detected needs to be known to build a reasonable optical model for fitting structural parameters. To determine the penetration depth of our measurement technique, we measured the reflectance spectra from a piece of nacre formed by Haliotis rufescens, then performed cross-sectional scanning electron microscopy (SEM) measurements of the full thickness of the nacre stack. The full ~3300-layer nacre stack was modeled about a hundred layers at a time, starting from the surface (i.e., first 100 layers, then 200 layers, etc.) using SEM thickness measurements for each layer. The modeled reflectance spectra were compared to reflectance measurement at the cross-section location to determine the penetration depth. Figure S3 shows the normalized calculated reflectance spectra of the nacre as the number of layers is increased. The curve in black is a measured normalized reflectance spectrum from a site adjacent to the cross-sectioned area. Figure S3b shows that the simulated reflectance spectra with the best fit to the measured reflectance occurs within the top 400 layers of nacre. A similar test was performed on a sectioned piece of Haliotis iris with the best fit occurring for the top 148 layers of nacre shown in figure S3c,d). For HIT optical modeling, we used a penetration depth of 200 layers for both species since this value is well within the range of good fits for MTT for both species and helped reduced the computational load.

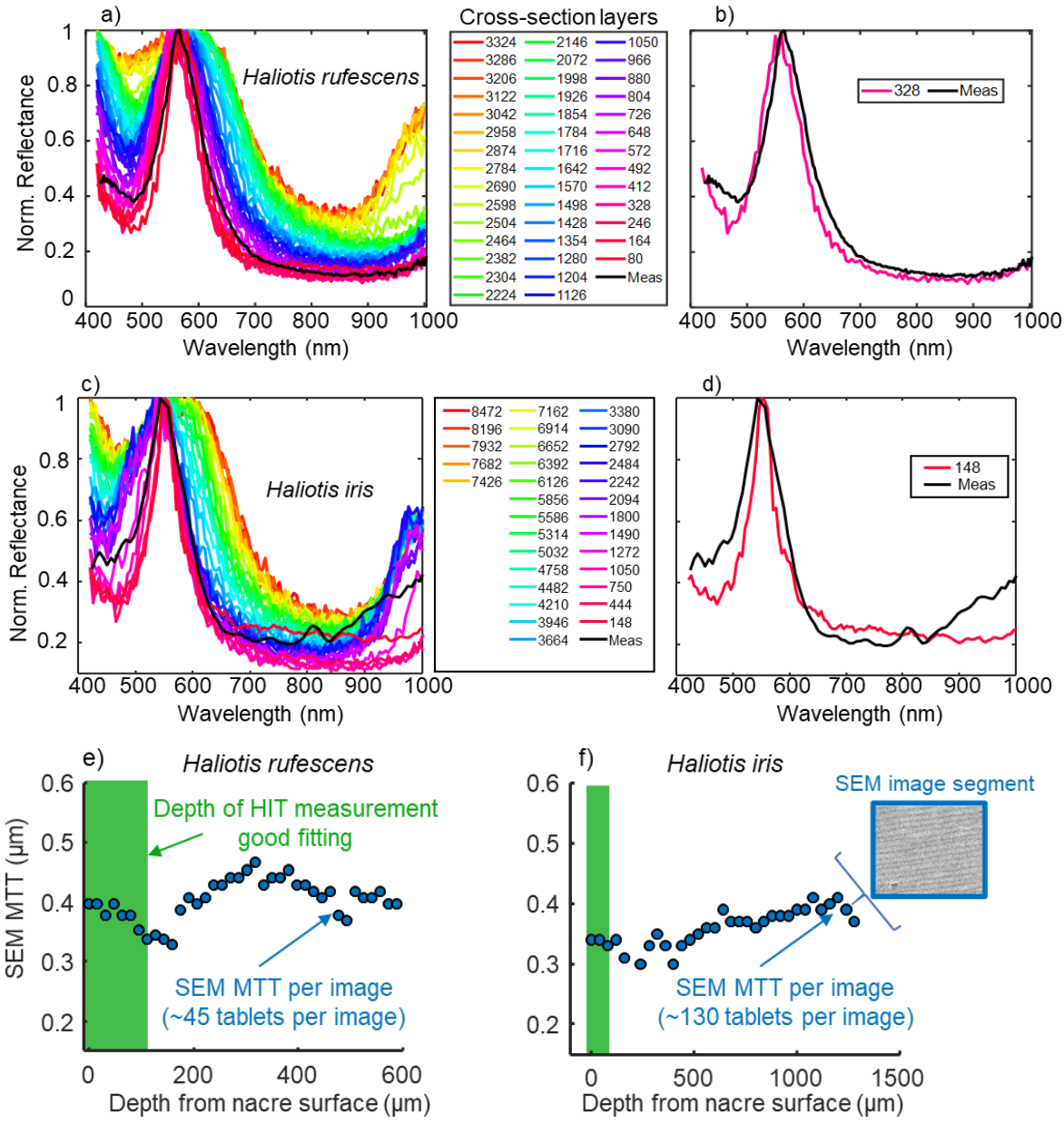

Figure S3: Simulation of thin-film assemblies of Nacre. a) Transfer-matrix-method calculation of the reflectance of a nacre thin-film assembly as layers are sequentially added to the model based on true cross-sectioned measurements of the tablet thicknesses formed by *Haliotis rufescens* (see section Supplementary sections 4 and 7). The first red line includes the top 80 layers of nacre, and so on until the entire nacre stack is simulated which includes over 3300 layers. In black, a normalized measured reflectance taken immediately adjacent to the cross-section cut (i.e., in the same location as the SEM measurements of the layer thicknesses). b) The simulated best-fit reflectance occurs when modeling about 330 layers in the stack. c) Simulated reflectance based on a sectioned piece of *Haliotis iris* with the normalized measured reflectance at the sectioned location overlaid in black. d) The corresponding best fit for this sample occurs at about 150 layers. e,f) Mean tablet thickness values measured from each imaged segment of the SEM

cross section (represented in inset (f)) as a function of depth from the nacre surface. Each image segment is comprised of ~45 (in e) or 130 (in f) tablets. The green rectangle highlights the depth to which HIT can measure for each sample based on the best fits from b,d).

In Fig. S3e,f we highlight the depth to which HIT penetrates (green box) based on the best fitting between the modeled spectra calculated from SEM-measured tablet thicknesses and the HIT measurement at the same location. We note that the full nacre stack has variations in tablet thicknesses extending beyond the depth which our current method can resolve (as seen with the blue dots from SEM measurements in Fig. S3e,f). While ideally—i.e., with no scattering, losses in the material, and totally planar surfaces—the full nacre stack would contribute to features to the total specularly reflected spectrum (as shown in full-stack calculations, orange lines in Fig. S3a,c), the expectation is that most nacreous or other biological structures will have significant scattering, nonuniformities, and possibly absorbing impurities that would all reduce the depth for which light can penetrate.

Furthermore, as has been shown for sufficiently disordered dielectric layered media, the localization of light can cause the intensity of transmitted light to decrease exponentially through the structure (S1) potentially limiting the depth which can be analyzed.

Therefore, a priori knowledge of the measurement depth of HIT in the underlying structure of any new species—as demonstrated in this section—would allow for the most accurate analysis. However, we emphasize that HIT can be used without knowledge of the measurement depth by fitting to only the high-reflectance bands in nacre. As noted in the main text, MTT correlates directly with the wavelength positions of the band peaks, while disorder correlates with the band broadening and is affected by the number of layers penetrated. Thus, an iridescent, nacre-like structure can still have the mean tablet thicknesses mapped, but the MTT values will represent information based on an unknown volume of the structure.

4. SEM measurements of the distribution of nacre tablet thicknesses

The optical model used in HIT assigns the aragonite tablet thickness values randomly from a Gaussian distribution centered at a given mean value and standard deviation (given by the degree of disorder). To confirm the distribution of tablet thicknesses is indeed Gaussian, we extracted the individual tablet thicknesses via cross-sectional SEM measurements on a piece of nacre formed by *Haliotis rufescens*. Figure S4 shows the entire cross-sectioned region and highlights the area where individual layer thicknesses were measured. Image processing of the SEM data measured edge-to-edge spacing between individual tablets. A histogram plot shows that the distribution of the tablet thicknesses at this location on the shell is approximately Gaussian, with a mean centered at 420 nm and a standard deviation of 50 nm.

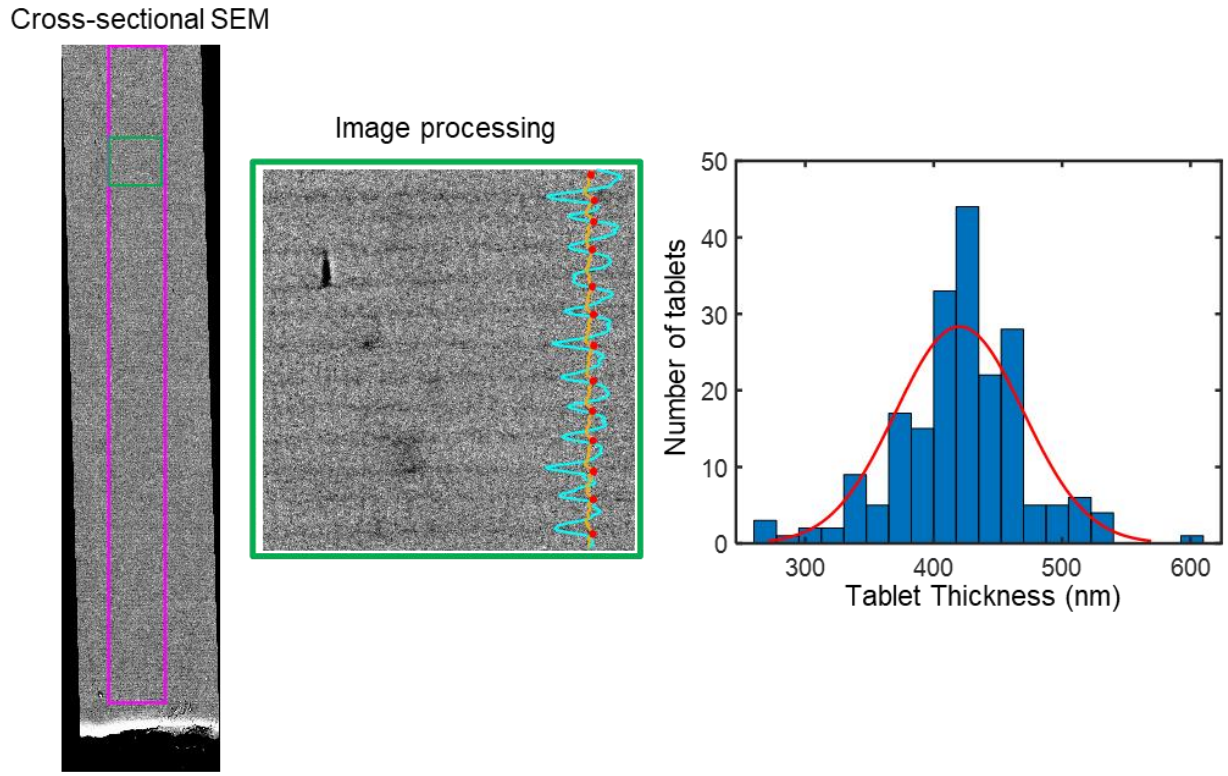

Figure S4: Nacre tablet distribution validation. (left) A composite cross-sectional SEM image of a nacre stack from a sample of *Haliotis rufescens*. The pink rectangle highlights the region where individual nacre tablets are counted, and thicknesses measured. (center) The inset shows a close-up region of nacre tablets defined by the green box. Image processing of the pixel intensities allow for individual tablets to be resolved by calculating edge-to-edge differences (shown as intensity profiles (cyan line), intensity derivative (orange line), and points of maximum slope (red dots)). (right) A histogram of the measured tablets in the cross-section. The tablets have a Gaussian distribution of thicknesses centered around a mean of 420 nm with a standard deviation of 50 nm.

5. Fitting of thickness from spectral data

To a first order, nacre can be modeled as a disordered Bragg reflector. As described in the main text, we combined transfer-matrix-method calculations with the Monte Carlo method to simulate 91×14 ensemble spectra given inputs of aragonite mean tablet thickness, MTT (150 – 600 nm), and degree of disorder in tablet thickness, which is the standard deviation, σ (5 – 70 nm) (see Fig. 2 in main text). Fitting was done pixel by pixel to determine the best fit between the simulated and measure spectra. The fitting procedure entails several steps and was performed computationally using MATLAB.

First, all measured and simulated spectra were normalized to their peak reflectance values, which was set to 1 (Fig. S5a, black line). The normalization eliminated discrepancies in absolute reflectance magnitudes. The most critical spectral features are preserved and correlate strongly with the MTT. The band broadening, which is an indicator of nacre tablet disorder, is also preserved. After normalization, the spectra are smoothed using a moving-average function with a 10-point average to eliminate high-frequency fluctuations in the spectra from measurement noise (Fig. S5a, gray line). Then, numerical differentiation of the smoothed spectra is calculated with respect to the wavelength. The derivative of the measured

reflectance for each pixel in our hyperspectral maps is compared to the derivate of all simulated reflectances (91 × 14 simulated ensemble spectra) using a mean-squared error (MSE) calculation. The simulated spectrum that has the lowest MSE value is considered the best-fit and its corresponding MTT and σ are recorded (Fig. S5b).

A second refinement fit is done using the initial best-fit parameters as a starting point. The MSE is calculated between original measured reflectance spectra and all simulated spectra within 20 nm of the initial best-fit MTT and σ. The fit parameters that produce a spectrum with the lowest MSE are chosen as the final best fit for the specific pixel (Figure S5c).

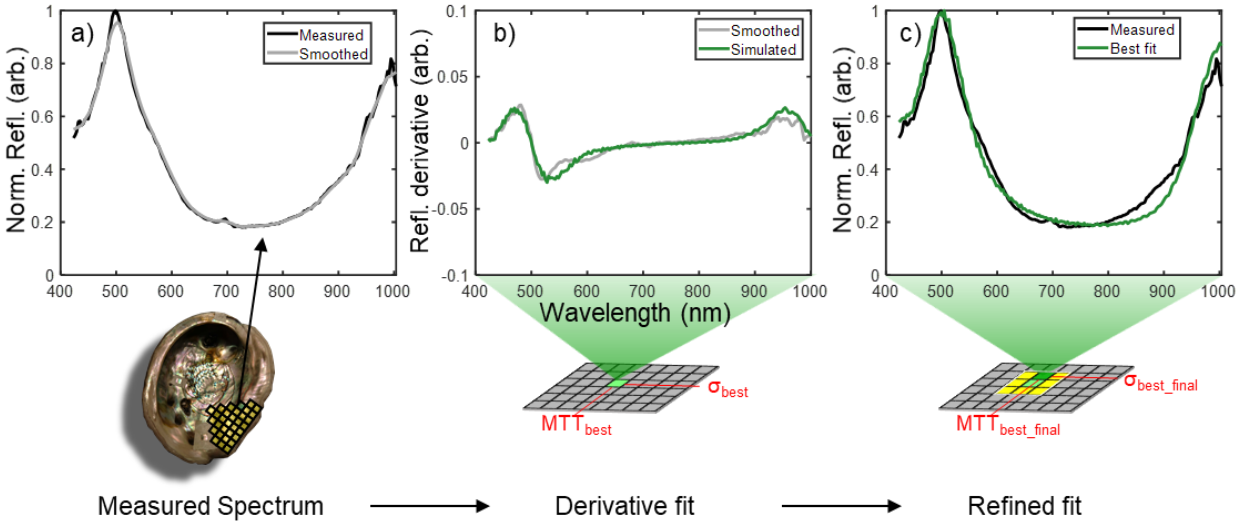

Figure S5: Refined MTT and σ fitting method. a) A measured reflectance spectrum from a single point along the nacre shell is normalized to the peak reflectance (black line). The spectrum is then smoothed using a 10-point moving average to reduce noise (grey line). b) The derivative of the smooth spectrum is compared to the derivatives of all 91 × 14 ensemble simulated spectra until the lowest mean-squared error is found between the two spectra. An initial MTT_{best} and σ_{best} is found. c) A second fitting is done within a subset of the simulation parameter space (white box with yellow squares). The space is defined as all spectra which are within 20 nm of the initial MTT_{best} and σ_{best} determined in (b). The final fitting is a direct comparison of normalized measured and simulated reflectance spectra. The final refined fit is selected and assigned to the point on the mapped shell.

The purpose of the double fitting method—with the first fitting based on the derivative of the reflectance and the second fitting based on the direct spectra—is to improve the reliability of fitting to points on the nacre with noisy, low-intensity spectra. As shown in Fig. S6a-c, fitting directly to spectra yielded reliable fits to measurements with clean and high-intensity spectra, *i.e.*, regions with strong specular reflectance. However, direct fitting often failed to reasonably fit to measured spectra that clearly have Bragg reflectance bands but are noisy due to a low-intensity specular component. Therefore, by first taking the derivative of the smoothed spectra, noise was reduced and baseline offsets in the spectra were removed, leaving primarily the spectral features of interest—the high-reflectance bands—for fitting. The fitting of noisy, weak reflectance spectra was significantly improved with the introduction of the derivative fit.

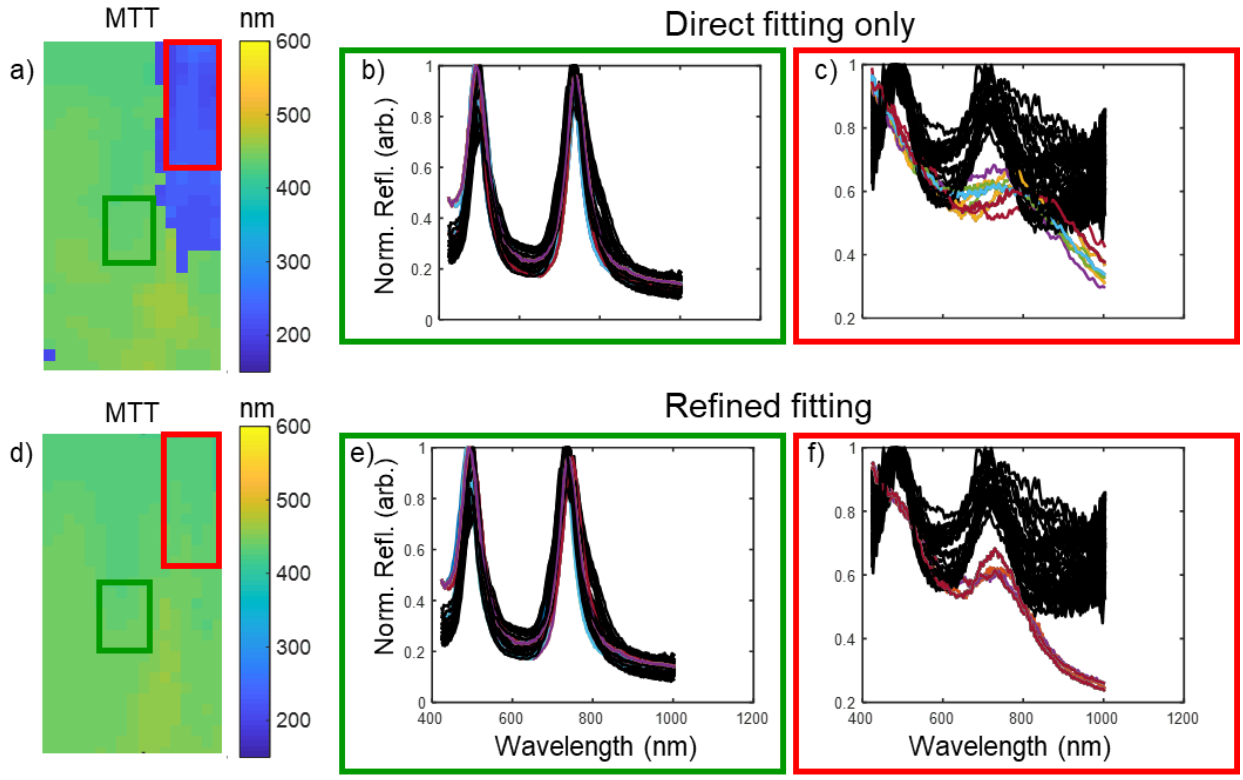

Figure S6: Comparison of single versus refined fitting. a) A mean tablet thickness (MTT) map based on a direct fitting of measured (black lines) and simulated (colored lines) reflectance spectra. In the map, a stark shift in the MTT is noted between the green and red highlighted regions. b) The best fits from the green highlighted region have good agreement between measured and simulated spectra. The measured spectra have clearly defined features with low noise—indicative of strongly specular reflectance. However, the red highlighted region has poor agreement with high variability in the fits due to increased noise from the weakly specular measurements. d) By fitting to the derivative of the spectra first, followed by a refined direct fit of spectra, the artificial discontinuities (dark blue regions versus light green regions) in the MTT maps are eliminated. e) High-quality fits are maintained for strongly specular data, while for noisy spectra (f), better fitting is achieved.

6. Details of scrubbed fitting maps for thickness and disorder

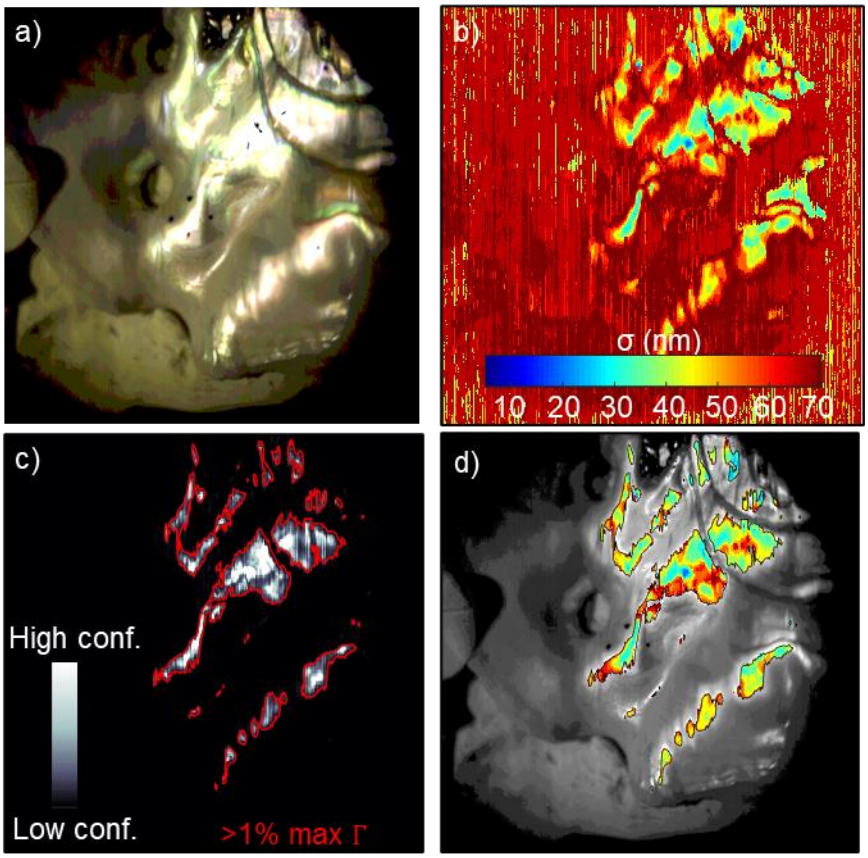

Figure S7: Scrubbed degree of disorder in tablet thickness (σ) maps. a) A color rendered image of a section of a 135-mm-long red abalone shell. After fitting, the best-fit MTT (Figure 3) and σ maps (b) are extracted. c) A map of the figure-of-merit confidence, Γ, is shown. (d) An overlay of our scrubbed σ map and a greyscale photo of the measured area.

7. SEM validation cross-sections

Sections of the largest abalone shell were cut with a TechCut 4™ precision low-speed saw (Allied High Tech Products, Rancho Dominguez, CA, USA), being careful to preserve the two analyzed regions described in Fig. 4 in the main text. A notch was made in the shell to identify specific regions on the shell where direct comparisons could be made. After the desired cross section was cut, that section of the shell was analyzed with the hyperspectral camera and the mean tablet thickness was calculated via the methods described above. The shell was then embedded cut-side down in Solarez ® UV resin (Wahoo International, Vista, CA, USA) in a 1" round mold. The resin was cured for 15 minutes with UV light (Jaxman U1c Flood flashlight) at a wavelength of 365 nm. The cross section was ground with 320, 400, 600, and 1000 grit SiC paper (Buehler, Lake Bluff, IL) and polished with 300 nm and then 50 nm alumina suspensions (Buehler, Lake Bluff, IL), dialyzed against 22 g/L Na_2CO_3 in DI H_2O solution before polishing, and the 22 g/L Na_2CO_3 solution was also added onto the polishing felt regularly during polishing to prevent dissolution of the $CaCO_3$. The polished sample was cleaned using TexWipe® Cotton (Texwipe, Kernersville, NC), air dried, and coated in 20 nm Pt using a Cressington 208 Series sputter coater (Cressington Scientific Instruments, Watford, England) equipped with a thickness monitor while spinning and tilting. The SEM cross-sections were analyzed in backscattered electron (BSE) mode with a Hitachi S3400 variable pressure

scanning electron microscope, located in the Ray and Mary Wilcox SEM lab in the University of Wisconsin-Madison Department of Geosciences.

Table S2: Resulting SEM MTT and σ measurements compared to fitted values from hyperspectral mapping.

Site	SEM MTT (nm)	Fitted MTT* (nm)	SEM σ (nm)	Fitted σ (nm)	Number of tablets measured in cross section
1	391	395	40	40	159
2	376	390	39	40	182
3	378	395	38	40	97

* 25 nm is added to all fitted values to account for the organic binding polymer. SEM measurement do not allow us to discriminate between the aragonite and the organic layers.

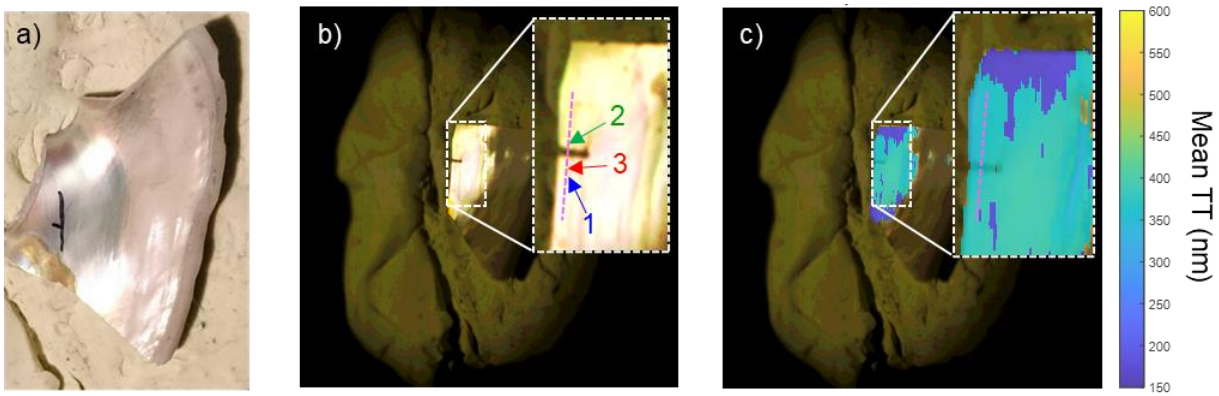

Figure S9: Cross-sectional scanning electron microscopy validation of nacre MTT and σ. a) A color image of the sectioned piece of red abalone nacre. The original shell size is 135 mm corresponding to the oldest mollusk in our data set. The black pen mark with notch demarks the region of interest for dicing and sectioning. b) A color-rendered image taken from the hyperspectral map of the nacre post dicing. An approximate 1 mm notch is made to easily identify the measurement location under the SEM. The measurement regions of interest are noted as site 1, 2, 3 and are recessed from the saw edge. The pink dashed line demarks the new edge and region of measurement after embedding the material and polishing the saw mark. c) An overlay of the MTT map on top of the color rendered image. The top 100 – 200 layers from the nacre surface were used to calculate the MTT thickness from the SEM measurements. This is representative of the depth of nacre our hyperspectral mapping method probes.

8. Dependence of nacre tablet disorder with age

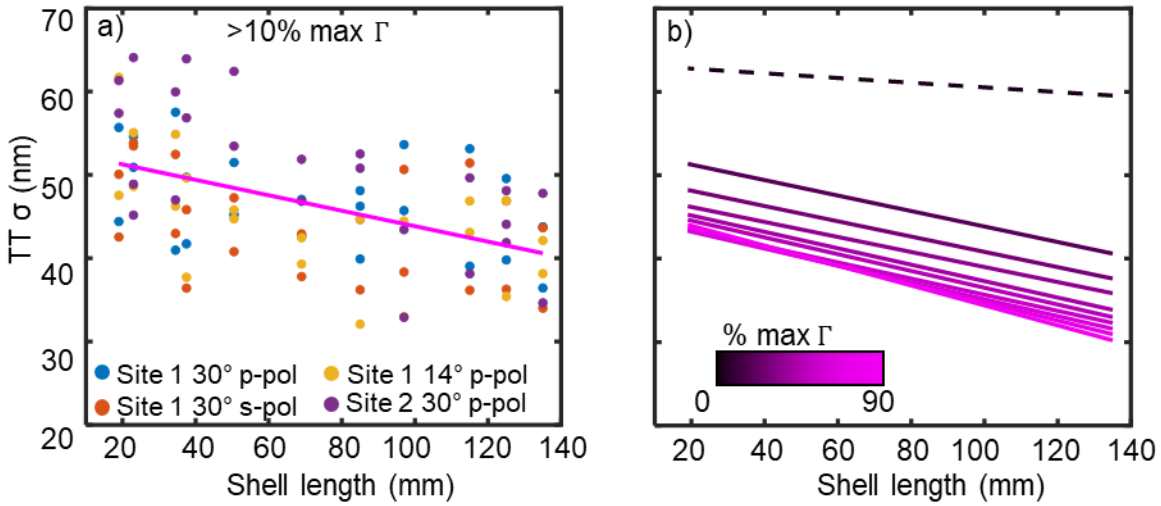

Figure S10: Ontogenetic dependence of degree of disorder (σ) in tablet thickness (TT) of red abalone. a) A plot showing fitted degree of disorder for all sample sites measured across 22 red abalone shells as described in the main article. An inverse relationship with shell size, which correlates to the age of the mollusk, can be seen with the linear fit to the average thickness for each group (pink dashed line). The threshold for data included in this specific plot is for any results with a Γ greater than 10% of the maximum Γ. b) Plots of linear-fit trends obtained selecting different scrubbing thresholds, with black representing unscrubbed data, and the lightest magenta representing datasets scrubbed with a minimum Γ threshold set to 90% of the peak Γ for each map.

9. Size and MTT dependence on age

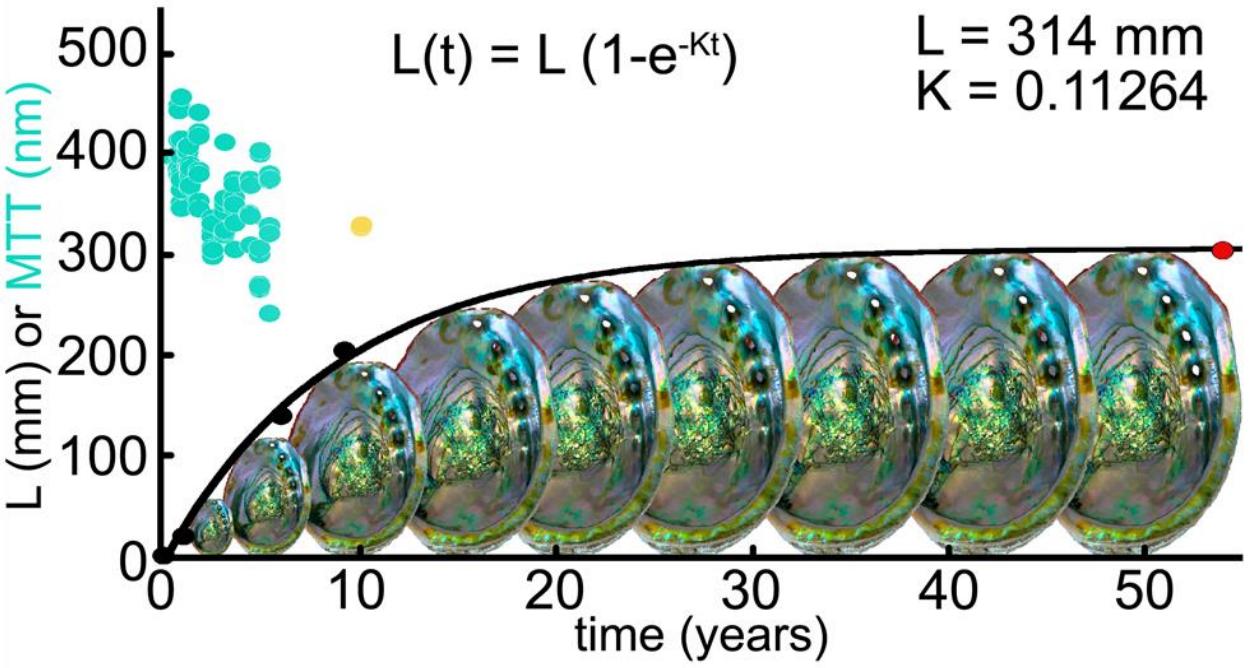

Figure S11: Red Abalone growth and mean tablet thickness (MTT) dependence on shell age. A plot shows the shell size dependence on time—or shell age—after fitting to a von Bertalanffy function (black line), which is an exponential rise describing the growth rate of animals. The red dot corresponds to the oldest and largest sized red abalone. In aqua green are the HIT-measured MTT data versus age extracted from the Bertalanffy function The yellow MTT data point is measured from a 205 mm red abalone shell with an unknown growth history and environmental temperature. It was not harvested at the same time or location as all other samples in this work, but is consistent with the other scattered data points. A photo of red abalone is repeated and scaled to visually represent the shell size variation with age.

All animals grow faster when they are young than when they are old. This growth behavior follows a von Bertalanffy curve (S2), described by the exponential function $L(t) = L[1 - e^{-Kt}]$, where L(t) is the length of the shell (or any other animal size parameter), t is time or age, and L and K are species-specific constants. In Fig. S11, the black curve is fit to the von Bertalanffy function using four age datapoints (0, 1, 6, and 54 years). The oldest and thus the largest of our samples was 6 years old. We included a further data point at 54 years based on the oldest age the *Haliotis rufescens* species can live (S3) and the largest size it can grow (S4) (red dot in Fig. S11). Including this red dot in the von Bertalanffy fit, we obtained the best fit parameters indicated in the plot: L = 314 mm and K= 0.11264.

Using the von Bertalanffy fit, we inferred the ages of all shells measured in this work and plotted their measured MTT versus time (aqua green dots in Fig. S11).

Red abalone, as all other nacre-forming mollusks, was expected to deposit tablet layers of identical thicknesses throughout its lifetime, and to deposit more layers per unit time when it was younger and progressively fewer as it grew in size and age. The observation that the thickness of the layers, instead, decreases with age is unexpected and interesting.

Movie S1: Columnar nacre stacking. 3D rendering of the structure of columnar nacre found in gastropods such as abalone. Each nacre tablet is a single crystal of aragonite, with the shape of an irregular polygon forming a Voronoi construction in each tablet layer. Each color corresponds to a different crystal c-axis orientation, highlighting co-orientation of all tablets within a column, and the column-to-column variation of the crystal orientations—and therefore refractive indices—within nacre. Column-to-column colors are similar because all c-axis orientations in nacre are spread within a 30° angle. Tablet layers are nearly equally spaced; thus nacre behaves as a (somewhat disordered) 1D Bragg reflector, which allows tablet thickness to be measured using Hyperspectral Interference Tomography (HIT). The animation was created using Blender from https://www.blender.org/.

S1. T. M. Jordan, J. C. Partridge, N. W. Roberts, Disordered animal multilayer reflectors and the localization of light. *Journal of The Royal Society Interface* **11**, 20140948 (2014).

S2. A. J. Fabens, Properties and fitting of the von Bertalanffy growth curve. *Growth* **29**, 265–289 (1965).

S3. Life History Information for Selected California Marine Invertebrates and Plants (September 25, 2020).

S4. Haliotis rufescens | MARINe (September 25, 2020).